High-Performance Control for a Bearingless Permanent Magnet Synchronous Motor Using Neural Network Inverse Scheme plus Internal Model Controllers

Xiaodong Sun, *Member, IEEE*, Long Chen, Haobin Jiang, Zebin Yang,
Jianfeng, Chen, and Weiyu Zhang

Abstract—This paper proposes a novel decoupling scheme for a bearingless permanent magnet synchronous motor (BPMSM) to achieve fast-response and high precision performances and to guarantee the system robustness to the external disturbance and parameter uncertainty. The proposed control scheme incorporates the neural network inverse (NNI) method and 2-degree-of-freedom (DOF) internal model controllers. By introducing the NNI systems into the original BPMSM system, a decoupled pseudo-linear system can be constituted. Additionally, based on the characteristics of the pseudo-linear system, the 2-DOF internal model control theory is utilized to design extra controllers to improve the robustness of the whole system. Consequently, the proposed control scheme can effectively improve the static and dynamic performances of the BPMSM system, as well as adjust the tracking and disturbance rejection performances independently. The effectiveness of the proposed scheme has been verified by both simulation and experimental results.

Index Terms—Bearingless permanent magnet synchronous motor (BPMSM), decoupling control, internal model control, neural network inverse (NNI).

I. INTRODUCTION

Permanent magnet synchronous motors (PMSMs) have been extensively investigated and applied all over the world due to its advantages of simple structure, reliable operation, high

efficiency, high torque density and power density, high robustness, reasonable cost, suitable for high speed, etc [1]-[4]. However, there may be many issues when the mechanical bearings are employed to bear the high-speed shaft of PMSMs [5]. On the one hand, the utilization of mechanical bearings can lead to the problems of heavy friction and wear [6], which may not only cause inefficiency of motors and short lifespan of the mechanical bearings but also increase the maintenance of motors. On the other hand, in some extreme conditions such as vacuum and fluid pumps in chemical and biochemical, pharmaceutical, and semiconductor industries, where an ultrahigh cleanness has to be guaranteed, the lubrication oil that is required by mechanical bearings cannot be used.

To effectively solve these problems caused by mechanical bearings, magnetic bearings are researched and developed [7], [8]. The technique of magnetic bearings is an ingenious solution to the problems of mechanical bearings since it has the advantages of no friction, no abrasion, no lubrication, maintenance-free operation, high durability, high speed and high precision, and lower shear stress and heat generation [9]. However, high power density of the motors with magnetic bearings is difficult to implement due to its complex structure and increased axial length of the rotor [10].

One of the solutions to overcome the shortcoming of magnetic bearings can be bearingless motors [11]. A bearingless motor is a magnetically integrated machine with the functions of both rotation and noncontact magnetic suspension. Bearingless permanent magnet synchronous motors (BPMSMs), having torque and suspension force windings in the stator, can be designed with high efficiency, high torque density and power density, reliable operation, compact size, and reasonable cost. BPMSMs have demonstrated the potential applications in turbomolecular pumps, centrifugal machines, high-speed precision mechanical processing, compressors, aeronautics and astronautics, flywheel energy storage, semiconductor industries, life science, etc [12].

The traditional linear control scheme, i.e., the proportional-integral-differential (PID) control scheme, are usually preferred but due to their fixed proportional gain (K_p), integral time constant (T_i), and differential time constant (T_d), the performance of the PID control scheme can be affected by

parameter variations, load disturbances and speed variations [13], [14]. Therefore, it is very difficult for this linear control scheme to obtain a sufficiently high-performance control for the BPMSM system which is a multivariable, nonlinear, and strongly coupling system with the time-variance of plant parameters as well as unavoidable disturbances.

If a nonlinear system can be equivalent to a linear one, the control of the nonlinear system is immensely simplified. Consequently, we can make use of all kinds of mature control strategies to design appropriate closed loop controllers for the simplified system. So far, inverse system method has been widely used in decoupling control of nonlinear systems [15], [16]. We can construct the inversion of the nonlinear system, and then cascade it with the original system to achieve the decoupling control of the nonlinear system. Nevertheless, the accurate mathematical models of the controlled plants are prerequisite when the inverse system method is employed. Due to the complexity of the BPMSM system, its mathematical model cannot be obtained precisely. Hence, the purpose of decoupling control is difficult to achieve by only utilizing the inverse system theory. The other approaches are needed to combine with the inverse system theory to realize the decoupling control.

As neural network technology is advancing fast, its applications in different fields are expanding rapidly [17]-[19], including combined with inverse system theory to construct a neural network inverse (NNI) system [20], [21]. In [20], the NNI control scheme is adopted by M. Xu *et al*. to achieve the decoupling control of a bearingless synchronous reluctance motor, and the expert PID controllers are employed for the pseudo-linear system. However, only the decoupling control between the radial suspension displacements in x- and y-directions is carried out, and the decoupling control among radial displacements and speed are not yet considered. In addition, only some simple simulation researches are studied in [20], and the further experimental studies are not performed. In [21], with regard to the control issue of a bearingless induction motor, Z. Wang and X. Liu adopt the NNI control and internal model control method, and some simulation and experimental researches are carried out. However, the traditional internal model control used in [21] has only one degree-of-freedom (DOF). It is obvious that the utilization of a filter to detune the controller imposes the tradeoff of sacrificing control performance to obtain the robustness [22].

Up to now, there is rare literature concerning the control issue of the BPMSM system by adopting the NNI plus internal model control scheme. Since the developed pseudo-linear system of the BPMSM by using the NNI control scheme is not a simple linear system, the uncertainties, unmodeled dynamics, and parameters variations may inevitably influence the properties of decoupling, tracking, disturbance rejection and robustness. The traditional internal model control can obtain good performance for set point tracking, but gives the sluggish response for disturbance rejection problem. That is to say, it is difficult for traditional internal model control to give consideration to both tracking and disturbance rejection properties [23]. Therefore, for purpose of improving the static

and dynamic properties of the whole BPMSM system, and adjusting the performances of tracking and disturbance rejection independently, the NNI control scheme plus 2- DOF internal model controllers are adopted in the paper.

The paper is arranged as follows. In Section II, the mathematical model of the BPMSM and its inversion will be deduced. In Section III, the NNI control scheme is employed for decoupling control of the BPMSM system, and then the 2-DOF internal model controllers are designed to improve system robustness. After that, simulation and experimental studies are performed to verify the effectiveness of the proposed control scheme in Section IV. Finally, the conclusions will be drawn in Section V.

II. INVERSE SYSTEM MODELING

A. Principle of Radial Suspension Force Generation

The torque winding (with pole pair P_M and radian frequency ω_M) and suspension force winding (with pole pair $P_B = P_M \pm 1$ and radian frequency $\omega_B = \omega_M$) are wound together in the same stator slots of the BPMSM to generate the torque and radial suspension force simultaneously. Subscripts M and B correspond to torque winding and suspension force winding, respectively (the same hereafter).

Fig. 1 shows the principle of the radial suspension force generation. As shown in Fig. 1, windings N_{Md} and N_{Mq} are 2-pole torque windings, and windings N_{Bd} and N_{Bq} are 4-pole suspension force windings. When the rotor is located in the center, the symmetrical 2-pole flux ψ_2 is generated by the torque winding current and PMs. If the BPMSM is driven at no load, the 2-pole fluxes produced by the of torque winding currents i_{Md} and i_{Mq} are small enough to be neglected. Under the condition that the suspension force winding current is zero, only the symmetrical 2-pole excitation flux linkage ψ_2 illustrated with the solid curves plus arrows is generated by the PMs, which causes the airgap flux density equal to each other in airgaps 1 and 3, and no radial suspension force is generated on the rotor. If the suspension force winding current i_{Bd} in the suspension force winding N_{Bd} exists as shown in Fig. 1, the symmetrical 4-pole suspension force flux ψ_4 shown with the dotted curves plus arrows is generated. As a result, the flux density is increased in the airgap 1 since the direction of the 4-pole suspension force flux ψ_4 is the same as that of the 2-pole excitation flux linkage ψ_2. On the contrary, the flux density is decreased in the airgap 3 for the direction of ψ_4 is opposite to ψ_2. Hence, the radial suspension force F_x, which tends to move the rotor to the positive x-direction, is generated, as shown in Fig. 1. A radial suspension force toward the negative direction in the x-axis can be produced with a negative current i_{Bd} in the suspension force winding N_{Bd}. Similarly, the radial suspension force F_y in the y-axis can be produced by the suspension force winding current i_{Bq} in the suspension force windings N_{Bq}. Therefore, radial suspension force $\boldsymbol{F}$ can be generated in any desired direction by a vector sum of F_x and F_y.
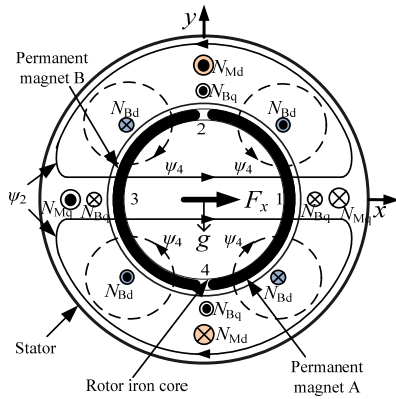
Fig. 1. Principle of the radial suspension force generation.

B. Description of the Mathematics Model

When the nonlinear magnetic saturation of magnet, the unbalance pull, and the iron losses are neglected, the theoretical formulae of the radial suspension forces and torque can be given as

$$\begin{cases} F_x = (K_M + K_L)(i_{Bd}\Psi_{Md} + i_{Bq}\Psi_{Mq}) \\ F_y = (K_M + K_L)(i_{Bq}\Psi_{Md} - i_{Bd}\Psi_{Mq}) \\ T = 3P_M(\Psi_{Md}i_{Mq} - \Psi_{Mq}i_{Md})/2 \end{cases} \quad (1)$$

where F_x and F_y are the suspension force components in x- and y-directions, respectively; i_{Bd} and i_{Bq} are current components of suspension force windings in d-q coordinate, respectively; $\Psi_{Md} = L_{Md}i_{Md} + \Psi_f$, and $\Psi_{Mq} = L_{Mq}i_{Mq}$ are the airgap flux linkages components of torque windings and PMs of rotor in the synchronously rotating d-q reference frame, respectively; Ψ_f is the equivalent excitation flux linkages of PMs; L_{Md} and L_{Mq} are the self-inductances of torque windings in the synchronously rotating d-q reference frame, respectively; i_{Md} and i_{Mq} are current components of torque windings in the synchronously rotating d-q reference frame, respectively; $K_M = \pi P_M P_B L_{m2}/(8lr\mu_0 W_M k_{WM} W_B k_{WB})$, and $K_L = 3P_M W_B k_{WB}/(4r W_M k_{WM})$ are Maxwell forces and Lorentz forces constants, respectively; P_M and P_B are the pole-pair numbers of torque and suspension force windings, respectively; L_{m2} is the mutual inductance of suspension force windings; l is the length of rotor iron core; r is the radius of the stator inner surface; W_M and W_B are the number of turns of torque and suspension force windings, respectively; k_{WM} and k_{WB} are winding factor of torque and suspension force windings, respectively.

According to the rotor dynamics and Newton's second law, the dynamic model of system motion equations can be written as

$$\begin{cases} m\ddot{x} = F_x \\ m\ddot{y} = F_y - mg \\ J\dot{\omega}/P_M = T - T_L \end{cases} \quad (2)$$

where x and y are the radial displacements in x- and y-directions, m is mass of the rotor, g is the gravity constant, J is the moment of inertia of the rotor, ω are speed of rotor, and T and T_L are the electromagnetic torque and the load torque, respectively.

C. Analysis of the Invertibility of the BPMSM

The objective of the proposed control scheme is to decouple the rotational speed ω and the radial displacements x and y in x- and y-directions. Hence, ω, x and y are chosen as the outputs of the BPMSM system, and output variables are $Y = [y_1, y_2, y_3]^T = [x, y, \omega]^T$. In addition, choose the suspension force winding current components i_{Bd} and i_{Bq}, and the torque winding current components i_{Md} and i_{Mq} to be the input variables, then $U = [u_1, u_2, u_3, u_4]^T = [i_{Md}, i_{Mq}, i_{Bd}, i_{Bq}]^T$. Choose ω, x, y, and the first derivative of x and y to be the state variables, then $X = [x_1, x_2, x_3, x_4, x_5]^T = [x, y, \dot{x}, \dot{y}, \omega]^T$. Consequently, (2) can be rewritten as

$$\dot{X} = f(X, U)$$

$$= \begin{bmatrix} \dot{x}_1 \\ \dot{x}_2 \\ \dot{x}_3 \\ \dot{x}_4 \\ \dot{x}_5 \end{bmatrix} = \begin{bmatrix} x_3 \\ x_4 \\ \dfrac{K_M + K_L}{m}\left(L_{Md}u_1u_3 + \Psi_f u_3 + L_{Mq}u_2u_4\right) \\ -\dfrac{K_M + K_L}{m}\left(L_{Md}u_1u_4 + \Psi_f u_4 - L_{Mq}u_2u_3\right) - g \\ \dfrac{3}{2J}P_M^2\Psi_f u_2 - \dfrac{P_M}{J}T \end{bmatrix} \quad (3)$$

According to the inverse system theory and *Interactor* algorithm, the outputs of the system are differentiated until the derivatives contain input U obviously

$$\dot{y}_1 = \dot{x}_1 = x_3 \quad (4)$$

$$\ddot{y}_1 = \ddot{x}_1 = \dot{x}_3 = \frac{K_M + K_L}{m}\left(L_{Md}u_1u_3 + \Psi_f u_3 + L_{Mq}u_2u_4\right) \quad (5)$$

$$\dot{y}_2 = \dot{x}_2 = x_4 \quad (6)$$

$$\ddot{y}_2 = \ddot{x}_2 = \dot{x}_4 = -\frac{K_M + K_L}{m}\left(L_{Md}u_1u_4 + \Psi_f u_4 - L_{Mq}u_2u_3\right) - g \quad (7)$$

$$\dot{y}_3 = \dot{x}_5 = \frac{3}{2J}P_M^2\Psi_f u_2 - \frac{P_M}{J}T \quad (8)$$

Thus, the Jacobi matrix can be resolved as

$$A(X, U) = \begin{bmatrix} \dfrac{\partial \ddot{y}_1}{\partial u_1} & \dfrac{\partial \ddot{y}_1}{\partial u_2} & \dfrac{\partial \ddot{y}_1}{\partial u_3} & \dfrac{\partial \ddot{y}_1}{\partial u_4} \\ \dfrac{\partial \ddot{y}_2}{\partial u_1} & \dfrac{\partial \ddot{y}_2}{\partial u_2} & \dfrac{\partial \ddot{y}_2}{\partial u_3} & \dfrac{\partial \ddot{y}_2}{\partial u_4} \\ \dfrac{\partial \dot{y}_3}{\partial u_1} & \dfrac{\partial \dot{y}_3}{\partial u_2} & \dfrac{\partial \dot{y}_3}{\partial u_3} & \dfrac{\partial \dot{y}_3}{\partial u_4} \end{bmatrix} =$$

$$\frac{K_M + K_L}{m}\begin{bmatrix} L_{Md}u_3 & L_{Mq}u_4 & L_{Md}u_1 + \Psi_f & L_{Mq}u_2 \\ -L_{Md}u_4 & L_{Mq}u_3 & L_{Mq}u_2 & -L_{Md}u_1 - \Psi \\ 0 & \dfrac{3mP_M^2\Psi_f}{2(K_M + K_L)J} & 0 & 0 \end{bmatrix}$$

$$(9)$$

Obviously, rank[$A(X, U)$]=3 and the matrix $A(X, U)$ is nonsingular. Moreover, the relative orders of the system are: $\alpha=(\alpha_1,\alpha_2,\alpha_3)=(2, 2, 1)$, which satisfy $\alpha_1+\alpha_2+\alpha_3 = 5 \leq n$ (is the number of the state variables). Thus, it can be concluded that the inverse of the original system is existent. According to implicit function theorem, the inverse system can be written as:

$$U = [u_1, u_2, u_3, u_4]^T == \xi(X, y_1, \dot{y}_1, \ddot{y}_2, y_2, \dot{y}_2, \ddot{y}_2, y_3, \dot{y}_3) \quad (10)$$

III. NNI-Based Internal Model Control Strategy

Even if the inverse of the BPMSM system has been obtained, it is still difficult to get its exact expression. Moreover, there are lots of parametric perturbations, unpredictable disturbances, and unmodeled dynamics in the practical application, the robustness and anti-disturbance often cannot meet the requirements. Therefore, NNI and internal model control theories will be introduced to improve these problems in this section.

A. Back-Propagation Neural Networks

There are many different types of neural networks, and one neural network which has received most attention in the field of engineering applications is the feed-forward neural network with the back-propagation (BP) learning algorithm, i.e., BP neural network. A BP neural network consists of a number of interconnected processing elements, commonly referred to as neurons, which are often grouped into input, hidden and output layers. Each neuron is connected to all the neurons in the next layer, and it has weighted inputs, summation function, transfer function and output. The transfer functions of neurons primarily determine the behavior of a BP neural network. The summation function is computed from the weighted sum of all input neurons, and its expression can be given as:

$$\text{net}_j^k = \sum_i w_{ji} O_i^{k-1} \quad (11)$$

where net_j^k is the summation function of the j-th neuron in the k-th layer, w_{ji} is the weight from the i-th neuron in the (k-1)-th layer to the j-th neuron in the k-th layer and O_i^{k-1} is the output of the i-th neuron in the (k-1)-th layer.

The activation signal of the summation function can be treated as an input to the transfer function from which the output of the neuron is determined. The role of the transfer function is to translate the summed information into outputs. In this paper, a tangent function is employed as the transfer function. The output of the j-th neuron O_j^k for the k-th layer can be expressed as:

$$O_j^k = f(\text{net}_j^k) = \frac{e^{\text{net}_j^k} - e^{-\text{net}_j^k}}{e^{\text{net}_j^k} + e^{-\text{net}_j^k}} \quad (12)$$

The desired output T_j is compared with the actual output O_j, and the error E_p is computed, respectively, which can be expressed as:

$$E_p = \frac{1}{2}\sum_j (T_j - O_j)^2 \quad (13)$$

The connection weights are modified to reduce the error associated with the overall error function. In this paper, the gradient descent method plus a momentum term is utilized to minimize the error E between the desired and actual outputs of the BP neural network as rapidly as possible. The new incremental change of weight $\Delta w_{ji}(n+1)$ can be given as:

$$\Delta w_{ji}(n+1) = -\eta\frac{\partial E}{\partial w_{ji}} + \alpha\Delta w_{ji}(n) \quad (14)$$

where n is the index of iteration, α is the momentum coefficient and η is the learning rate. The BP neural network can memorize the relationship between the input and output vectors through the connection weights via this learning process.

B. NNI System

The BP neural network is utilized to approach the inversion of the BPMSM system, and five integrators are used to characterize its dynamic characteristics. The original BPMSM system is excited by the appropriate incentive signals of the suspension force and torque windings currents i_{Md}, i_{Mq}, i_{Bd}, and i_{Bq} in the actual operating area, and then the corresponding responses of radial displacements x and y, and speed ω can be obtained. Then, the input and output signals $\{i_{Md}, i_{Mq}, i_{Bd}, i_{Bq}, x, y, \omega\}$ of the original BPMSM system can be sampled. According to (10), the input signals of the inversion include radial displacements x and y and their 1-order and 2-order derivative, and speed and its 1-order derivative, and the output signals include suspension force and torque windings currents i_{Md}, i_{Mq}, i_{Bd}, and i_{Bq}. Therefore, the inputs and outputs of the neural network are $\{\ddot{x}, \dot{x}, x, \ddot{y}, \dot{y}, y, \dot{\omega}, \omega\}$ and $\{i_{Md}, i_{Mq}, i_{Bd}, i_{Bq}\}$. Regarding the differentiators appearing in the inputs of the neural network, it can be realized by using a five-point numerical differential algorithm to guarantee high computing accuracy.

After the derivatives $\{\ddot{x}, \dot{x}, x, \ddot{y}, \dot{y}, y, \dot{\omega}, \omega\}$ were gained by the five-point numerical differential algorithm, the training sample sets $\{\ddot{x}, \dot{x}, x, \ddot{y}, \dot{y}, y, \dot{\omega}, \omega\}$ and $\{i_{Md}, i_{Mq}, i_{Bd}, i_{Bq}\}$ of the neural network can be finally obtained. Before the beginning of the training process, both input and output variables should be normalized to obtain a usable form for the BP neural network to read.

According to the inputs and outputs of the BP neural network, it is easy to determine that the numbers of neurons in the input and output layers are 8 and 4, respectively. However it is not so easy to determine the appropriate number of neurons in the hidden layer since there is currently no definite rule to choosing it, and it is usually determined according to the experiments and researchers' experience. The average root-mean-square (RMS) error E_{RMS} between the actual output y_j and predicted output $\hat{y}_j$ is used to check the convergence criterion for the developed networks, and can be calculated with the following equation:

$$E_{RMS} = \frac{1}{p}\sum_{i=1}^{p}\sqrt{\frac{1}{n}\sum_{j=1}^{n}(y_{ji} - \hat{y}_{ji})^2} \quad (15)$$

where p and n are the numbers of training or testing data and variables in the output vector, respectively. The influence of number of neurons in hidden layer on the network performance is studied, which is shown in Table I. It can be seen that increasing the number of neurons in the hidden layer cannot

ensure the decrease of the average RMS error E_{RMS}. Therefore, from Table I, it can be obviously observed that the optimal number of the neurons in the hidden layer is 18.

TABLE I
INFLUENCE OF HIDDEN-LAYER NEURONS ON THE NETWORK PERFORMANCE

Configuration	Training E_{RMS}	Testing E_{RMS}
8-8-4	0.0667	0.0652
8-10-4	0.0658	0.0641
8-12-4	0.0663	0.0639
8-14-4	0.0657	0.0627
8-16-4	0.0652	0.0623
8-18-4	0.0634	0.0602
8-20-4	0.0662	0.0627
8-22-4	0.0659	0.0631
8-24-4	0.0648	0.0629
8-26-4	0.0659	0.0632

Then various parameters of the BP neural network, including the learning rate, momentum coefficient, and number of neurons in the hidden layer, can be optimized by trial-and-error. The learning rate can determine the changing speed of the weights, and the momentum coefficient can prevent the unexpected changes in obtaining the results. In this paper, the learning rate and momentum are set at 0.12 and 0.88 through experimentation, respectively. After approximate 800 epochs training, the training error of the BP neural network is under 0.001 and hence meeting the requirement. Therefore, the BP neural network is constructed successfully.

The trained BP neural network can then be used to implement the inversion of the original BPMSM system, and accordingly by cascading the NNI with original system, a pseudo-linear system can be built as illustrated in Fig. 2. The pseudo-linear system is equivalent to two 2-order and a 1-order linear integral subsystems. The developed scheme does not need the accurate model of the original system, and the robustness and anti-disturbance of the whole system can be improved greatly.
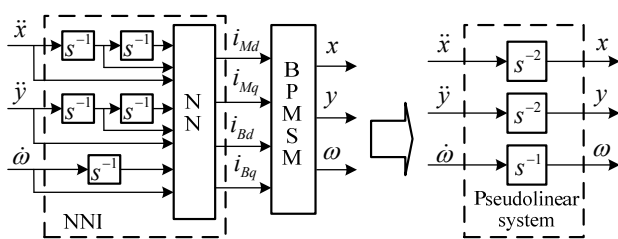

Fig. 2. Diagram of pseudo-linear system.

C. 2-Degree-of-Freedom Internal Model Controllers

It can be found from Fig. 2 that by cascading the NNI with the original BPMSM system, a simple open-loop pseudo-linear system is constituted. Thus, to achieve the high-performance control of the BPMSM system, the closed-loop controllers are the essential parts of the whole control system.

In this section, we will develop the 2-DOF internal model controllers for the open-loop pseudo-linear system. According to Fig. 2, two radial displacements and speed are decoupled, so controllers for three pseudo-linear subsystems are designed

independently. Taking the x- direction radial displacement as an example, Fig. 3 shows the structure of 2-DOF internal model controller, where $G(s)$ and $G_x(s)$ are the real plant to be controlled and the internal model, respectively, $G_{c1}(s)$ and $G_{c2}(s)$ are internal model controllers, x^* and x are the reference input and output of x- direction radial displacement, respectively, v is the control input, d_x is the outer disturbance input, and e is the error.
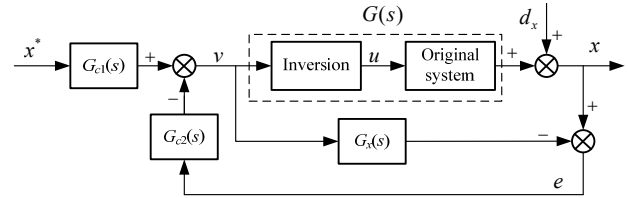

Fig. 3. The 2-DOF internal model controller structure.

The ideal transfer function of the pseudo-linear subsystem of x- direction radial displacement can be written as

$$G_x(s) = 1/s^2 \qquad (16)$$

The transfer function (16) is the nominal model of the radial displacement in x- direction of the BPMSM system. However, the composition of the actual control plant and its inversion (10) do not exactly equal to the linear subsystem (16) due to the existence of model errors and unmeasurable disturbances. The actual transfer function of the pseudo-linear subsystem, including the uncertainties and noises, can be expressed as

$$G(s) = G_x(s) + G_d(s) \qquad (17)$$

where $G_d(s)$ denotes an arbitrary uncertainty.

From Fig. 3, we can calculate the output as

$$x(s) = \frac{x^*(s)G_{c1}(s)G(s) + d_x(s)(1 - G_{c2}(s)G_x(s))}{1 + G_{c2}(s)G_d(s)} \qquad (18)$$

If the internal model is accurate, i.e., $G_x(s) = G(s)$, (18) can be rewritten as

$$x(s) = x^*(s)G_{c1}(s)G_x(s) + d_x(s)(1 - G_{c2}(s)G_x(s)) \qquad (19)$$

From (19), we can see that the tracking performance only depends on $G_{c1}(s)$, while the disturbance rejection property only relies on $G_{c2}(s)$. To track the reference input x without any steady-state error as well as to enhance the system robustness, the internal model controller $G_{c1}(s)$ and $G_{c2}(s)$ are designed as

$$\begin{cases} G_{c1}(s) = G_x^{-1}(s)Q_1(s) \\ G_{c2}(s) = G_x^{-1}(s)Q_2(s) \end{cases} \qquad (20)$$

where $Q_1(s)$ and $Q_2(s)$ are the low-pass filters, and can be commonly chosen as

$$\begin{cases} Q_1(s) = (1 + \lambda_1 s)^{-2} \\ Q_2(s) = (1 + \lambda_2 s)^{-2} \end{cases} \qquad (21)$$

where $\lambda_1 > 0$ and $\lambda_2 > 0$.

Moreover, by simplifying Fig. 3, we can obtain the improved 2-DOF internal model controller as depicted in Fig. 4. Here

$$\begin{cases} T(s) = \dfrac{G_{c1}(s)}{G_{c2}(s)} = \dfrac{(1+\lambda_2 s)^2}{(1+\lambda_1 s)^2} \\ G_c(s) = \dfrac{G_{c2}(s)}{1 - G_{c2}(s)G_x(s)} = \dfrac{s^2}{(1+\lambda_2 s)^2 - 1} \end{cases} \quad (22)$$
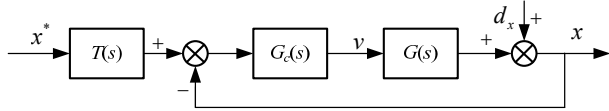

Fig. 4. The closed-loop system of the 2-DOF internal model controller.

The design process of the 2-DOF internal model controllers for the y- direction radial displacement shares the similar way. Moreover, the transfer function of the pseudo-linear subsystem of the rotor speed system is $G_\omega(s) = 1/s$. Thus, similarly, the corresponding 2-DOF internal model controllers can be designed as

$$\begin{cases} T'(s) = \dfrac{1+\lambda_2 s}{1+\lambda_1 s} \\ G_c'(s) = \dfrac{1}{\lambda_2} \end{cases} \quad (23)$$

D. Tracking, Disturbance Rejection, and Robustness Performances of the Designed 2-DOF Internal Model Controller

From Fig. 4, we can define the output error transfer function of the closed-loop system as

$$E(s) = x^*(s) - x(s)$$
$$= \frac{(1 + G_c(s)G(s)(1 - T(s)))x^*(s) - d_x(s)}{1 + G_c(s)G(s)} \quad (24)$$

To analyze the tracking performance, letting $d_x(s) = 0$ and $G(s) = G_x(s)$, then (24) can be written as

$$E(s) = (1 - Q_1(s))x^*(s) = \left[1 - (1+\lambda_1 s)^{-2}\right]x^*(s) \quad (25)$$

Similarly, to analyze the property of disturbance rejection, letting $x^*(s) = 0$ and $G(s) = G_x(s)$, then (24) can be written as

$$E(s) = -(1 - Q_2(s))d_x(s) = \left[(1+\lambda_2 s)^{-2} - 1\right]d_x(s) \quad (26)$$

According to (25) and (26), it can be concluded that the smaller λ_1, the better tracking performance, and the smaller the λ_2, the better the performance of disturbance rejection. In addition, it can also be drawn a conclusion that the closed-loop control system can track the step and sinusoidal signals without any steady-state errors, and can also reject the step and sinusoidal disturbance signals.

The necessary and sufficient condition for stabilization of the closed-loop system for arbitrary ω can be given as

$$\left| G_c(j\omega)G_x(j\omega) \right| \overline{l}_m < 1 \quad (27)$$

where $\overline{l}_m$ is the upper bound of the modeling error.

Substituting (16) and (20) into (27) yields

$$\left| (1+\lambda_2 s)^2 - 1 \right| > \overline{l}_m \quad (28)$$

From (28), it is obvious that for a certain modeling error upper bound $\overline{l}_m$, by selecting λ_2 appropriately, we can

guarantee the stability of the closed-loop system. In addition, we also can draw a conclusion that the larger the λ_2, the larger the $G_d(s)$ that can be acceptable.

Similarly, it can be proven that 2-DOF internal model controller for the rotor speed system is of the aforementioned characteristics.

According to aforementioned analysis of the system performance indexes and robust stability, we can realize the effective independent control of tracking and robustness performance by choosing an optimal control parameter sets λ_1 and λ_2. The control block diagram of the proposed 2-DOF internal model control based on NNI control scheme for the BPMSM system is given in Fig. 5.
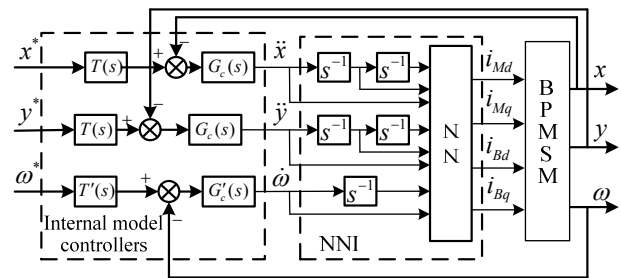

Fig. 5. Control block diagram of the entire system.

IV. SIMULATION AND EXPERIMENTAL RESULTS

To validate the efficient performance of the proposed control scheme, comparative simulation and experiments between the proposed control and the inverse system method plus PID controller have been performed. The system parameters and the parameters of the two control schemes are illustrated in Tables II-IV. The proposed control scheme is implemented in the Matlab/Simulink and a TMS320F2812 DSP-based control computer, respectively.

TABLE II
PARAMETERS OF THE PROTOTYPE MACHINE

Parameter	Value	Parameter	Value
P_M	1	P_B	2
r (mm)	67	R (mm)	65
l_m (mm)	2	l_g (mm)	1
l (mm)	85	N	24
W_M	40	W_B	40
k_{WM}	0.908	k_{WB}	0.955
Ψ_f (Wb)	0.0230	L_{m2} (mH)	3.27
J (kg·m^2)	0.00053	m (kg)	2.0

TABLE III
PARAMETERS OF THE 2-DOF INTERNAL MODEL CONTROLLER

Parameter	Value	Parameter	Value
λ_1	0.07 (0.03)	λ_2	0.04 (0.02)

TABLE IV
PARAMETERS OF THE PID CONTROLLER

Parameter	Value	Parameter	Value
K_p	18	K_i	26
K_d	0.45 (0.6)		

A. Decoupling Properties

In this part, to demonstrate the decoupling properties of the proposed control scheme, comparative simulation and experiments, including the speed step and the radial displacement step of the BPMSM system are carried out. The reference speed steps from 2500 r/min to 5000 r/min at $t = 0.4$ s, and then the reference radial displacement in x- direction increases from 0 to 40 μm at $t = 1.2$ s. Figs. 6 and 7 depict the comparative simulation and experimental results, respectively. In Figs. 6 and 7, from top to bottom are, in order, the speed, x- and y- axes radial displacements, respectively.
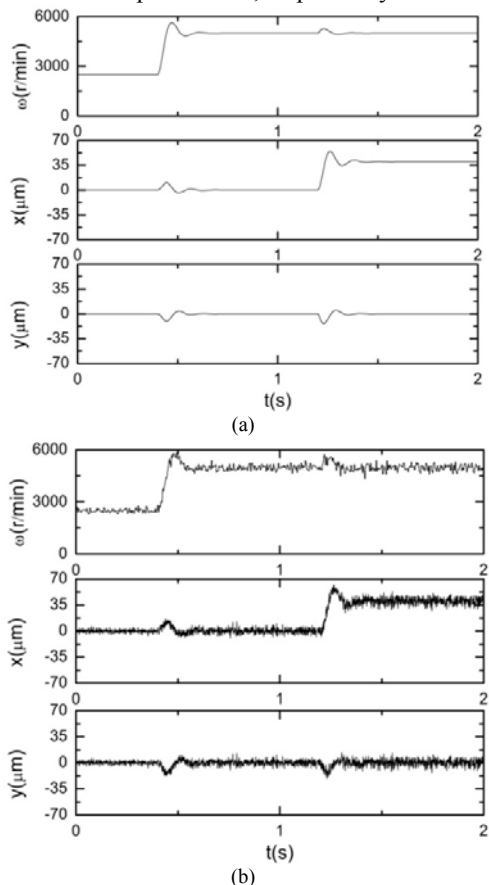

Fig. 6. Decoupling properties of the inverse system method plus PID controller. (a) Simulation results. (b) Experimental results.

As shown in Fig. 6 (a), when the speed reference suddenly steps from 2500 r/min to 5000 r/min at $t = 0.4$ s, as for the inverse system method plus PID controller, there are about 15 μm and 16 μm overshoots of the radial displacements in x- and y- directions, respectively. And there is about a 550 r/min overshoot of the speed response. However, as shown in Fig. 7 (a), compared with the inverse system method plus PID controller, the proposed control scheme has almost no fluctuations of the radial suspension system in x- and y- directions when the speed reference suddenly increases from 2500 r/min to 5000 r/min at $t = 0.4$ s. This demonstrates that there is strong coupling not only between the radial suspension system in x- and y- directions but also among the two radial suspension systems and the rotor speed one. On the contrary, compared with the inverse system method plus PID controller,

when the reference radial displacement in x- direction steps from 0 to 40 μm at $t = 1.2$ s, the proposed control scheme has almost no influence on the radial suspension system in y- direction and little disturbance to the rotor speed system. That is, a sudden change of one reference input has little influence on other two outputs, which indicates that by using the proposed control scheme, the decoupling control among the two radial suspension and rotor speed systems can be realized with great improvement on the response speed and control precision.
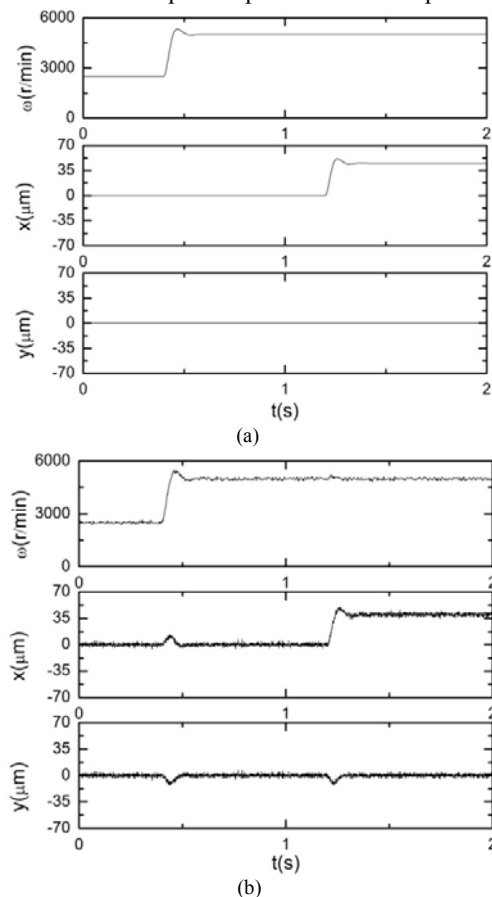

Fig. 7. Decoupling properties of the proposed control scheme. (a) Simulation results. (b) Experimental results.

Moreover, from Fig. 6 (b), it is obvious that when the inverse system method plus PID controller is adopted, with the change of the operating points, the steady-state peak-to-peak values of the rotor vibration amplitude in x– or y- direction increase from about 10 μm to 14 μm, and the steady-state peak-to-peak value of the speed increase from about 180 r/min to 500 r/min. On the contrary, according to Fig. 7 (b), we can see that when the proposed control scheme is employed, the steady-state peak-to-peak values of the rotor vibration amplitude in x– or y- direction and the speed are almost about 6 μm and 130 r/min, respectively, no matter whether the operating points change.

As shown in Figs. 6 and 7, it can be seen that the experimental results agree very well with the simulation ones. Since there are noises, static and dynamic imbalances in the physical BPMSM system, the control precision and adjusting time of the system may be inevitably affected. Thus, compared with the simulation results, the experimental ones are of

somewhat longer adjusting time, higher overshoot, and lower control precision. This can also be demonstrated in the latter studies.

B. Tracking, Disturbance Rejection, and Robustness Properties

In this part, in order to demonstrate the tracking, disturbance rejection, and robustness properties of the proposed control scheme, comparative simulation and experiments, including the speed step, external disturbance and parameter variation of the BPMSM system are carried out. At $t = 0$ s, the reference speed steps from 0 r/min to 6000 r/min. After 1 s, a 2 N·m radial disturbance is imposed on the magnetically suspended rotor, and at $t = 1.5$ s, the Maxwell force constant K_M decreases by 15%. Moreover, to further compare the performance of the two control schemes, different control parameters were developed too, as illustrated in Figs. 8 and 9.
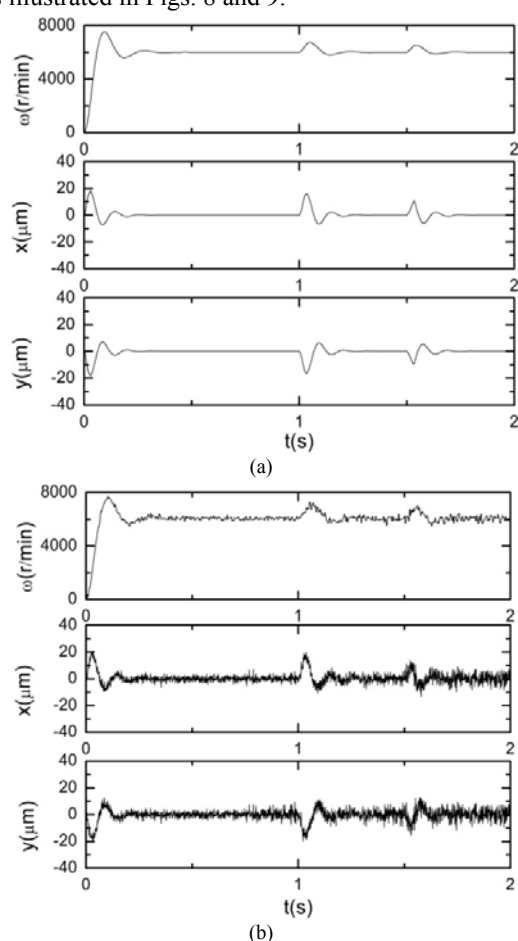

Fig. 8. Tracking and disturbance rejection properties of the inverse system method plus PID controller with $k_d = 0.5$. (a) Simulation results. (b) Experimental results.
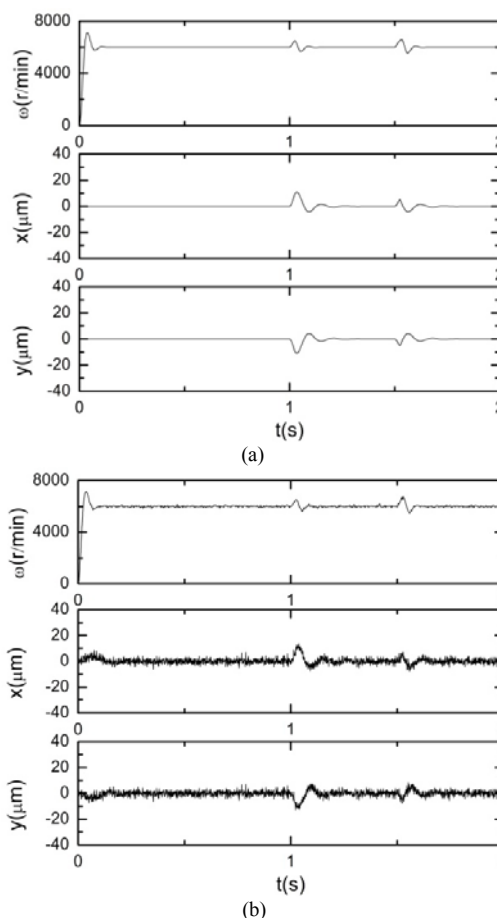

Fig. 9. Tracking and disturbance rejection properties of the proposed control scheme with $\lambda_1 = 0.062$ and $\lambda_2 = 0.038$. (a) Simulation results. (b) Experimental results.

In order to compare the simulation and experimental results systematically, here we define some important performance indexes and see how these performance indexes vary when the control parameters of the system change. In regard to the speed step of the rotor system, we choose the setting time and overshoot as the key indexes. With respect to the disturbance rejection and robustness properties, we choose the setting time and deviation value as the two main indexes. Note that the deviation value denotes the maximal deviating value from the steady-state position as an external disturbance or parameter variation occurs.

From Fig. 8 (a), it can be seen that with respect to the inverse system method plus PID controller, when the reference speed steps from 0 r/min to 6000 r/min at $t = 0$ s, there is approximate 1800 r/min fluctuations from the reference speed inputs (that is, the overshoot is 30%) with a 0.16s long setting time. In addition, when a 2 N·m radial disturbance is imposed on the magnetically suspended rotor at $t = 1$ s, the deviation value and setting time of the speed are respectively 800 r/min and 0.11 s, and the deviation values and setting times of radial displacements are respectively 18 μm and 0.12 s. When the Maxwell force constant K_M suddenly changes at $t = 1.5$ s, the deviation value and setting time of the speed are respectively 700 r/min and 0.1 s, and the deviation values and setting times

of radial displacements are respectively 16 μm and 0.11 s. In contrast, according to Fig. 9 (a), regarding proposed control scheme, the speed tracking curves are relatively steady with tiny overshoots (or deviation values) and short setting times when the reference speed step, external disturbance and parameter variation occurs, which undoubtedly indicates the superiority in the tracking, disturbance rejection, and robustness properties to the inverse system method plus PID controller.

In addition, according to the experimental results shown in Figs. 8 (b) and 9 (b), similar conclusions can be drawn, which are in good agreement with the simulation and the aforementioned analysis.

Here, taking the rotor speed as an example, a more specific comparison between the inverse system method plus PID controller and the proposed scheme is shown in Table V, where the aforementioned performance indexes change when the control parameter k_d of the inverse system method plus PID controller and the control parameters λ_1 and λ_2 of the proposed control method vary.

TABLE V
COMPARATIVE RESULTS BETWEEN TWO CONTROL SCHEMES WITH PARAMETERS VARYING

		Inverse system		Proposed scheme		
		$k_d =$ 0.5	$k_d =$ 0.75	$\lambda_1 =$ 0.062 $\lambda_2 =$ 0.038	$\lambda_1 =$ 0.062 $\lambda_2 =$ 0.016	$\lambda_1 =$ 0.024 $\lambda_2 =$ 0.016
Tracking	Setting time	0.16s	0.21s	0.07s	0.07s	0.05s
	Overshoot	30%	25%	20%	20%	10%
Disturbance rejection	Setting time	0.11s	0.11s	0.05s	0.04s	0.04s
	Deviation value	800 r/min	750 r/min	300 r/min	200 r/min	200 r/min
Robustness	Setting time	0.1 s	0.1 s	0.06s	0.04s	0.04s
	Deviation value	700 r/min	600 r/min	350 r/min	250 r/min	250 r/min

From Table V, it can be seen that, as for the inverse system method plus PID controller, when the value of the k_d increases from 0.5 to 0.75, the settling time of the speed response increase no matter whether there is an external disturbance or parameter variations. In contrast, the overshoots of the speed response decrease.

Thus, in regard to the inverse system method plus PID controller, we can draw a conclusion that it cannot adjust the tracking performance and the disturbance rejection performance independently. Hence, since the modeling errors always exist, it is quite difficult for the inverse system method plus PID controller to find out the optimized control coefficients when its operating points change. That is, even if the optimized control coefficients of the inverse system method plus PID controller can be selected sometimes, it cannot satisfy the tracking, disturbance rejection properties simultaneously.

However, regarding the proposed control scheme, the decrease of the values of λ_1 and λ_2 can both decrease the setting times and the overshoots of the speed response. Concretely speaking, by decreasing the control parameters λ_2, we can improve the disturbance rejection and robustness properties without any influences on the tracking property. On the other

hand, by decreasing the control parameters λ_1, we can enhance the tracking performance without any influences on the disturbance rejection and robustness properties. Therefore, it can be concluded that the proposed control scheme can adjust the tracking and disturbance rejection properties independently, which is in accordance with the analysis in section 3. Similarly, the same conclusion for the radial displacements in x- and y-directions can be drawn.

Obviously, the aforementioned simulation and experimental results demonstrate that, compared with the inverse system method plus PID controller, the proposed NNI control scheme plus internal model controller has great improvements on the high precision, fast response, and strong robustness, which can enhance the system stability and the static as well as dynamic properties of the whole BPMSM system significantly.

V. CONCLUSION

The BPMSM is a multivariable, strongly coupled and nonlinear system with unavoidable parameter variations and unmeasured disturbances. To effectively reject the nonlinear and coupling influence as well as to enhance the control properties of high-precision, fast-response, and strong-robustness for the BPMSM system, this paper proposes a new decoupling control scheme combing the NNI control method and the 2-DOF internal model controllers. The simulation and experimental results demonstrate that: (1) The NNI control scheme can successfully realize decoupling control of the BPMSM system; (2) By employing the 2-DOF internal model controllers based on the NNI control scheme, the unmodeled dynamics to the decoupling accuracy can be eliminate effectively; (3) By adjusting the control parameters λ_1 and λ_2, the tracking and disturbance rejection properties can be regulated independently.

REFERENCES

[1] B. M. Ebrahimi and J. Faiz, "Configuration impacts on eccentricity fault detection in permanent magnet synchronous motors," *IEEE Trans. Magn.*, vol. 48, no. 2, pp. 903-906, Feb. 2012.
[2] M. Morawiec, "The Adaptive backstepping control of permanent magnet synchronous motor supplied by current source inverter," *IEEE Trans. Ind. Inf.*, vol. 9, no. 2, pp. 1047-1055, May 2013.
[3] G. Lei, C. Liu, J. Zhu, and Y. Guo, "Techniques for multilevel design optimization of permanent magnet motors," *IEEE Trans. Energy Convers.*, vol. 30, no. 4, pp. 1574-1584, Dec. 2015.
[4] G. Lei, T. Wang, Y. Guo, J. Zhu, and S. Wang, "System-Level Design Optimization Methods for Electrical Drive Systems: Deterministic Approach," *IEEE Trans. Ind. Electron.*, vol. 61, no. 12, pp. 6591-6602, Dec. 2014.
[5] E. Estupinan and I. Santos, "Controllable lubrication for main engine bearings using mechanical and piezoelectric actuators," *IEEE/ASME Trans. Mechatronics*, vol. 17, no. 2, pp. 279-287, Apr. 2012.
[6] M. Riera-Guasp, J. A. Antonino-Daviu and G. Capolino, "Advances in electrical machine, power electronic, and drive condition monitoring and fault detection: state of the art," *IEEE Trans. Ind. Electron.*, vol. 62, no. 3, pp. 1746-1759, Mar. 2015.
[7] J. Abrahamsson, M. Hedlund, T. Kamf, and H. Bernhoff, "High-speed kinetic energy buffer: optimization of composite shell and magnetic bearings," *IEEE Trans. Ind. Electron.*, vol. 61, no. 6, pp. 3012-3021, Jun. 2014.
[8] C. Liu and G. Liu, "Equivalent damping control of radial twist motion for permanent magnetic bearings based on radial position variation," *IEEE Trans. Ind. Electron.*, vol. 62, no. 10, pp. 6417-6427, Oct. 2015.

[9] K. Jiang, C. Zhu and L. Chen, "Unbalance compensation by recursive seeking unbalance mass position in active magnetic bearing-rotor system," *IEEE Trans. Ind. Electron.*, vol. 62, no. 9, pp. 5655-5664, Sep. 2015.

[10] X. Sun and H. Zhu, "Neuron PID control for a BPMSM based on RBF neural network on-line identification," *Asian J. Control*, vol. 15, no. 6, pp. 1772-1784, Nov.2013.

[11] X. Sun, L. Chen, Z. Yang, and H. Zhu, "Speed-sensorless vector control of a bearingless induction motor with artificial neural network inverse speed observer," *IEEE/ASME Trans. Mechatronics*, vol. 18, no. 4, pp. 1357-1366, Aug. 2013.

[12] X. Sun, L. Chen and Z. Yang, "Overview of bearingless permanent-magnet synchronous motors," *IEEE Trans. Ind. Electron.*, vol. 60, no. 12, pp. 5528-5538, Dec. 2013.

[13] G. Andrikopoulos, G. Nikolakopoulos and S. Manesis, "Advanced nonlinear PID-based antagonistic control for pneumatic muscle actuators," *IEEE Trans. Ind. Electron.*, vol. 61, no. 12, pp. 6926-6937, Dec. 2014.

[14] K. H. Ang, G. Chong and Y. Li, "PID control system analysis, design, and technology," *IEEE Trans. Control Syst. Technol.*, vol. 13, no. 4, pp. 6975-6985, Jul. 2005.

[15] X. Dai, D. He, and T. Zhang, "MIMO system invisibility and decoupling control strategies based on ANN αth-order inversion," *IEE Proc.–Control Theory Appl.*, vol. 148, no. 2, pp. 125–136, Mar. 2001.

[16] J. Fang and Y. Ren, "Decoupling control of magnetically suspended rotor system in control moment gyros based on an inverse system method," *IEEE/ASME Trans. Mechatronics*, vol. 17, no. 6, pp. 1133-1144, Dec. 2012.

[17] X. Fu, S. Li and I. Jaithwa, "Implement optimal vector control for LCL-filter-based grid-connected converters by using recurrent neural networks," *IEEE Trans. Ind. Electron.*, vol. 62, no. 7, pp. 4443-4454, Jul. 2015.

[18] E. Kayacan, E. Kayacan and M. A. Khanesar, "Identification of nonlinear dynamic systems using type-2 fuzzy neural networks-a novel learning algorithm and a comparative study," *IEEE Trans. Ind. Electron.*, vol. 62, no. 3, pp. 1716-1724, Mar. 2015.

[19] S. K. Mondal, J. Pinto and B. K. Bose, "A neural-network-based space-vector PWM controller for a three-level voltage-fed inverter induction motor drive," *IEEE Trans. Ind. Appl.*, vol. 38, no. 3, pp. 660-669, May/Jun. 2002.

[20] M. Xu, X. Diao, D. Feng, and H. Zhu, "The neural network inverse decoupling control of bearingless synchronous reluctance motor," in *Proc. 32nd Chin. Control Conf.*, 2013, pp. 3259-3263.

[21] Z. Wang and X. Liu, "Nonlinear internal model control for bearingless induction motor based on neural network inversion," *Acta Automat. Sinica*, vol. 39, no. 4, pp. 433-439, Apr. 2013.

[22] D. Campos-Gaona, E. L. Moreno-Goytia and O. Anaya-Lara, "Fault ride-through improvement of DFIG-WT by integrating a two-degrees-of-freedom internal model control," *IEEE Trans. Ind. Electron.*, vol. 60, no. 3, pp. 1133-1145, Mar. 2013.

[23] S. Saxena and Y. V. Hote, "Load frequency control in power systems via internal model control scheme and model-order reduction," *IEEE Trans. Power Syst.*, vol. 28, no. 3, pp. 2749-2757, Aug. 2013.

Long Chen received the B.Sc. and Ph.D. degrees in mechanical engineering from Jiangsu University, Zhenjiang, China, in 1982 and 2006, respectively.

He is currently a Professor with the Automotive Engineering Research Institute, Jiangsu University. His areas of interest include electric vehicles, electric drives, simulation and control of vehicle dynamic performance, vehicle operation, and transport planning.

Haobin Jiang received the B.Sc. degree from Nanjing Agricultural University, China, in 1991, and the M.Sc. and Ph.D. degrees from Jiangsu University, China, in 1994 and 2000, respectively, in mechanical engineering.

He is currently a Professor with the Automotive Engineering Research Institute, Jiangsu University. His areas of interest include electric vehicles, vehicle dynamics performance analysis, and electronic control technologies for vehicles.

Zebin Yang received the B.Sc., M.Sc., and Ph.D. degrees in electrical engineering from Jiangsu University, China, in 1999, 2004, and 2013, respectively.

He is currently an Associate Professor with the School of Electrical and Information Engineering, Jiangsu University. His research interests include bearingless motors and magnetic bearing, and intelligent control of special motors.

Jianfeng Chen received the B.Sc. and M.Sc. degrees in electrical engineering from Jiangsu University, China, in 2002, and 2005, respectively, and Ph.D. degree in control engineering from Southeast University, China, in 2015.

Since 2002, he has been with Jiangsu University, where he is currently an Associate Professor with the Automotive Engineering Research Institute. His research interests include motor drives and control, strapdown inertial navigation, and intelligent control.

Xiaodong Sun (M'12) received the B.Sc. degree in electrical engineering, and the M.Sc. and Ph.D. degrees in control engineering from Jiangsu University, Zhenjiang, China, in 2004, 2008, and 2011, respectively.

Since 2004, he has been with Jiangsu University, where he is currently an Associate Professor with the Automotive Engineering Research Institute. From 2014 to 2015, he was a Visiting Scholar with the School of Electrical, Mechanical, and Mechatronic Systems, University of Technology Sydney, Sydney, Australia. His areas of interest include electrical machines and drives, drives and control for electric vehicles, and intelligent control.

Weiyu Zhang received the B.Sc. degree in control engineering and the Ph.D. degree in electrical engineering from Jiangsu University, China, in 2009 and 2014, respectively.

Since 2005, he has been with School of Electrical and Information Engineering, where she is currently a Lecturer. Her research interests include structure parameter design and control technology for magnetic bearings.